© smp chair committee (Kourosh Koushan and Sverre Steen)
DOI: 10.15480/882.9352

Eighth International Symposium on Marine Propulsors
smp'24, Berlin, Germany, March 2024

Propeller cavitation noise in hybrid viscous flow/FWH simulations using robust impermeable surface formulations

Joseph Praful Tomy[1,2], Keun Woo Shin[1], Stephan Berger[1,3], Max Steden[1], Harry B. Bingham[2], Poul Andersen[2]

[1]Propeller & Aft Ship Department, MAN Energy Solutions (MAN-ES), Denmark
[2]Technical University of Denmark, Kgs. Lyngby, Denmark
[3]FORCE Technology, Hydro- and Aerodynamics, Kgs. Lyngby, Denmark

ABSTRACT

The recent years have seen increasing interest in the numerical evaluation of the underwater noise from cavitating propellers. When Ffowcs-Williams-Hawkings (FWH) based acoustic analogy methods are extended to cavity surfaces, the adequacy of different formulations is still debatable. The acoustic sources may be defined on either impermeable (or non-porous or solid) data surfaces which coincide with physical body surfaces; or on a permeable data surface that encompasses the entire noise generating flow region. In a permeable-FWH approach, the acoustic solution is dependent on the porous enclosure selected; and there is no unanimous agreement about its extent. In a viscous finite volume solver with impermeable-FWH approach, the acoustic effects of cavity fluctuations are not completely captured, due to the absence of any physical cavity surface within the simulations. In this paper, a novel hybrid approach is investigated, wherein the accuracy of the cavitation flow dynamics from a viscous CFD solver is combined with the simplicity of an acoustic source definition using impermeable surfaces. The flow simulations are performed in Star-CCM+ using incompressible two-phase Detached Eddy Simulations (DES) and the Schnerr-Sauer cavitation model. The instantaneous cavity surface geometry is extracted from the simulation results and used to define equivalent acoustic sources. The acoustic predictions from the model are verified by comparing with hydrodynamic pressure pulses from DES. Finally, the results are compared with experimental measurements, in order to evaluate the performance of each method.

Keywords: permeable FWH, impermeable FWH, cavitation noise, underwater acoustics, URN

1 INTRODUCTION

Propeller cavitation is a vital phenomenon in the design of marine propulsion systems, characterized by the formation and collapse of vapor bubbles around the propeller due to the reduction of local pressure below the vapor pressure of water. The adverse effects of cavitation on ship propulsive efficiency and propeller blade durability have always been important concerns for propeller designers. Recent years have seen growing interest about cavitation-induced underwater noise of propellers. This underwater noise, often termed 'hydroacoustic noise', has gained increasing attention due to its far-reaching ecological impact on marine mammals and the overall health of aquatic environments.

Numerical modeling of propeller cavitation noise is an essential component of underwater acoustics research and engineering. Numerical models allow engineers and researchers to assess noise levels under various operating conditions, aiding in the design of quieter vessels and the implementation of noise-reduction strategies. However, this endeavor is filled with challenges, including accurately capturing the complex interactions between cavitation dynamics, fluid flow, and acoustic radiation. The computational effort required to numerically solve the compressible Navier-Stokes equations is in most cases prohibitive when dealing with the acoustics of propeller cavitation within an industrial context. To circumvent this, the Ffowcs-Williams-Hawkings (FWH) acoustic analogy method (Ffowcs-Williams and Hawkings 1969) is often employed, wherein the hydrodynamic flow solution from an incompressible solver is post-processed to obtain equivalent acoustic sources.

$$\begin{aligned}\Box^2 p' =& \frac{\partial}{\partial t}\{[\rho_0(v\cdot n)+\rho(u\cdot n - v\cdot n)]\delta(f)\} \\ &- \frac{\partial}{\partial x_i}\{[\Delta P_{ij} n_j + \rho u_i(u\cdot n - v\cdot n)]\delta(f)\} \\ &+ \frac{\partial^2}{\partial x_i \partial x_j}[T_{ij}H(f)]\end{aligned} \quad (1)$$

The FWH equation (1) is derived for a moving surface, $f(x,t) = 0$ enclosing the noise generating region of the flow. The acoustic pressure p' is represented as a sum of generalized function derivatives. $\Box^2$ represents the d'Alembert operator, δ represents the Dirac-delta function and H represents the Heaviside function. Subscripts i and j refer to the Einstein notation for tensor quantities. ρ_0 is the fluid density in the undisturbed fluid, ρ is the local fluid density, u is the local fluid velocity, v is the local surface velocity, and n is the unit surface normal vector. $\Delta P_{ij} n_j$ is the local force intensity vector, which contributes to the loading noise. T_{ij} is the Lighthill stress tensor, which contributes to the quadrupole noise. Equation (1) is the most generic form of the FWH equation, which is applicable to permeable (or porous) and impermeable (or non-porous or

solid) data surfaces. A solid data surface would result in a further simplification, with the local fluid velocity normal to the surface ($u \cdot n$) being equal to the local normal surface velocity ($v \cdot n$). The acoustic analogy implies that the noise contribution from within the region bounded by the surface can be modelled in terms of equivalent acoustic monopoles and dipoles on the surface. In case of solid data surfaces, the acoustic source terms on the right-hand side of the equation can be associated with physical definitions of thickness, loading and quadrupole noise sources respectively (Brentner and Farassat 2003).

The thickness source term models the noise generated due to fluid displacement. The loading source term models the noise due to unsteady loading on the solid surface. The quadrupole source term pertains to non-linearities in the flow-field due to high-speed transonic flow or high amount of turbulence (Testa 2008). For rotating propellers at low Mach number flow, the quadrupole noise term is often neglected to reduce the computational complexity, but not without controversy (Ianniello 2016). This is usually a reasonable assumption when the data surface encloses all the relevant noise sources (Brentner and Farassat 2003). The advantage of such a simplification is that the acoustic noise at any receiver location within the entire flow field can be calculated based on the knowledge of the flow field directly on the solid data surfaces. Consequently, the acoustic model can be represented by surface integral formulations such as the Farrassat1A formulation (Brentner and Farassat 2003).

The impermeable surface simplification to the FWH equation (hereafter referred to as solid-FWH), with acoustic sources placed only on the moving surface, is easier to implement and relevant for non-cavitating propeller flows. In the case of cavitating flow, this method requires a physical definition of the fluctuating cavity surface. Such acoustic models have previously been implemented using cavity surface definition based on the low-order potential based boundary element method (Göttsche et al. 2017). Viscous, finite-volume flow solvers do not inherently include the definition of such physical cavity surfaces. Non-viscous flow solvers include a computed definition of the cavity surface; but the cavitation dynamics is not captured accurately enough by the flow solver (Shin et al. 2015). It is for this reason that the general form of the FWH equation with a permeable data surface that encloses all the cavity sources (hereafter referred to as permeable-FWH) is frequently employed in viscous flow solvers to predict cavitating propeller noise. However, the acoustic solution in permeable-FWH is dependent on the porous enclosure selected (Lidtke et al. 2019); and there is no unanimous agreement about its extent (ITTC 2017; Ahmed 2020). A visual representation of the acoustic modelling approaches used by the permeable-FWH and solid-FWH models in the context of a cavitating hydrofoil is shown in Figure 1.

In this paper, a hybrid approach is investigated, wherein the accuracy of the cavitation flow dynamics from a viscous flow solver is combined with the simplicity of an acoustic source definition using solid-FWH. The flow simulations are performed using incompressible two-phase Detached Eddy Simulations (DES) in Star-CCM+. The instantaneous cavity surface geometry is extracted from the simulation results, and is used to define equivalent solid-FWH acoustic sources. The solid-FWH method provides a standardized definition for cavity acoustic sources; and its extent of applicability is investigated within this paper.

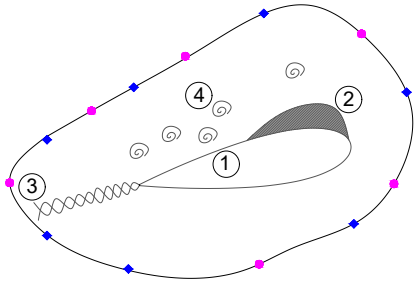

(a) Permeable-FWH formulation

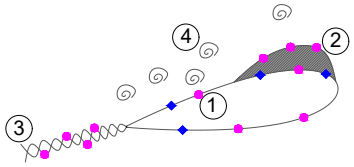

(b) Solid-FWH formulation

Hydrodynamic noise sources
1. Blade surface
2. Sheet cavity
3. Cavitating tip vortex
4. Flow turbulence

Acoustic analogy sources
- Monopoles
- Dipoles

Figure 1: Schematic representation of permeable-FWH and solid-FWH formulations for a cavitating hydrofoil

2 METHODOLOGY

This section provides details about the implementation of the solid-FWH model for the sheet cavity surface of a cavitating propeller. The methodology description is based on the case study of the 'Princess Royal' propeller, a five-bladed fixed pitch propeller of a twin-screw catamaran. The 'Princess Royal' propeller is used as a benchmark case for many propeller studies; the geometric details and vessel specifications are available in the public domain (Tani et al. 2017).

2.1 Flow Simulation Setup

The flow simulations are performed using the commercial Navier-Stokes solver, Star-CCM+. Turbulent viscous flow is simulated by the DES solver. Cavitating flow is modelled by the Volume of Fluid (VOF) method and the Schnerr-Sauer cavitation model. An unsteady simulation is made with the model scale propeller in a cylindrical fluid domain extending four propeller diameters ($4D$) to the inlet and six propeller diameters to the outlet from the propeller plane. Although a $4D$ radial extent of the fluid domain is sufficiently large, it is extended to $20D$ to investigate

the propagation of the hydrodynamic pressure. An inner cylindrical subdomain is defined around the propeller for modelling the propeller rotation as rigid body motion using a sliding grid. A trimmed hexahedral grid is prepared in the fluid domain. The CFD method adopted in this study has been validated against experimental results for different types of propeller cavitation and the setup details are found in Shin and Andersen (2019). The axial hull wake simulated in the cavitation tunnel test from Sezen and Atlar (2023) is applied to the propeller inflow in CFD. This is shown in Figure 2. The hull wake input is approximated to be symmetric and is applied to the inlet boundary. The flow simulation is performed at model scale, with the cavitation tunnel test setup. The model scale operating condition and its equivalent full scale values are shown in Table 1.

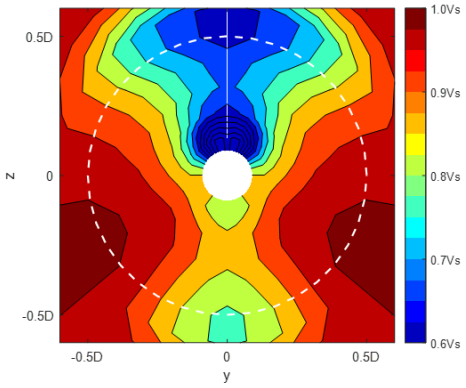

Figure 2: Axial hull wake applied to the propeller inflow in the flow solver. *Vs* is the ship speed, *D* is the propeller diameter.

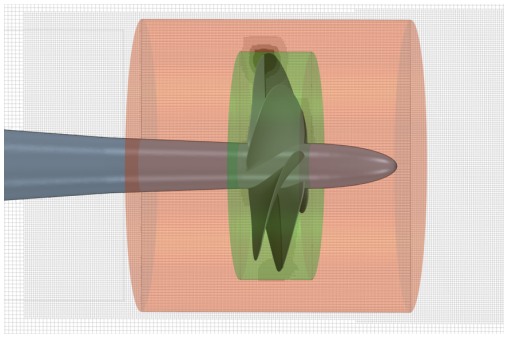

Figure 3: Propeller model in CFD with the volumetric grid on the vertical cross-section (green – noise source region in the permeable-FWH calculation, red – rotating subdomain)

Table 1: Simulation operating condition

Parameter	Full scale	Model scale
Propeller diameter [m]	0.75	0.25
Propeller speed [rps]	14.3	30
Engine RPM [rpm]	1500	—
Ship speed [m/s]	5.4	3.78
Cavitation number, σ_n	1.91	1.91
Thrust coefficient, K_T	0.225	0.219
Torque coefficient, $10K_Q$	0.323	0.317

2.2 Acoustic Models

There are two acoustic models used in the current study - the permeable-FWH model and the solid-FWH model. Both models are based on the FWH equation (1) for acoustic analogy of rotating surfaces. Both acoustic models assume an infinite field for sound propagation, i.e. the effects of reflecting boundaries such as the free surface, seabottom and ship hull have not been taken into account. The acoustic models are focused on investigating large-scale, coherent cavities. Small-scale cavitation phenomena, such as the growth and collapse of individual bubbles, is not captured by these models.

The solid-FWH model incorporating cavity surfaces is implemented within the in-house MAN-ES design code DOLPHIN. DOLPHIN is an acoustic solver based on the Farrassat1A formulation of the FWH equation. Originally developed as an acoustic analogy post-processing tool for a potential flow solver, the code has been adapted in this study to read input from Star-CCM+. The cavity normal velocities are used to define equivalent thickness noise sources in DOLPHIN. For the purpose of this study, only the noise from sheet cavities is considered; although, in principle, the same approach could be extended to tip vortex cavities. Based on an order of magnitude study for the current cavitating operating condition, the noise due to blade rotation is negligible compared to the cavitating noise, and hence not included in the current results. With reference to Figure 1(b), only the thickness noise sources on the cavity surface are included in the results of the current paper.

The permeable-FWH model is based on the inbuilt implementation in Star-CCM+, in which acoustic sources are defined on a permeable data surface. The acoustic domain (or the permeable data surface) is defined by a downstream cylindrical region inside the rotating domain for the permeable-FWH calculation as indicated by green in Figure 3. Permeable-FWH calculations using a similar setup have previously been published for a cavitating propeller in the behind-hull condition (Shin et al. 2023). Since the solid-FWH model within the current study does not include the acoustic effects of tip vortex cavities and other trailing vortices, it is justified to define the permeable surface in the permeable-FWH model closely surrounding the propeller blades, such that it encloses the sheet cavities. The equivalent acoustic monopoles and dipoles on the permeable data surface include the noise contributions within the acoustic domain, i.e. the blade surfaces, sheet cavities, and flow turbulence in the vicinity of the blades.

2.3 Cavity Surface Definition

The sheet cavity surface is not inherently defined in the finite volume CFD solver, and hence needs to be approximated. This approximation is achieved by defining an isovolume of cells that have a vapor-water volume fraction greater than 0.9. The cavity surface is defined as the exterior isosurface boundary of the isovolume. To process the results, segmental cuts are made on the isosurface along the blade radial direction. Figure 4 shows a collection of data points for a blade segment with representative cavitation, at $r = 0.9R$ and a blade angular position of 40 degrees.

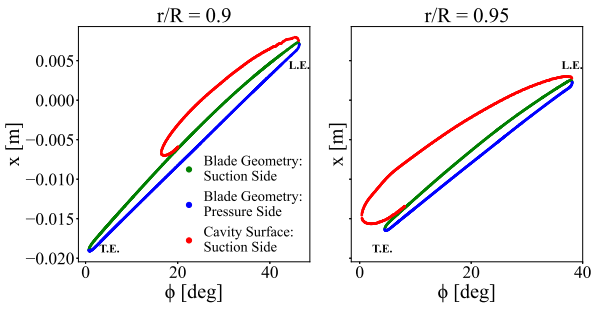

Figure 4: Blade surface and cavity surface geometries extracted from Star-CCM+, represented in a ship-fixed cylindrical coordinate system. Origin is at the propeller hub centre. x is positive in the propeller upstream direction, and ϕ is the angular coordinate in the clockwise direction from the 12 o'clock position.

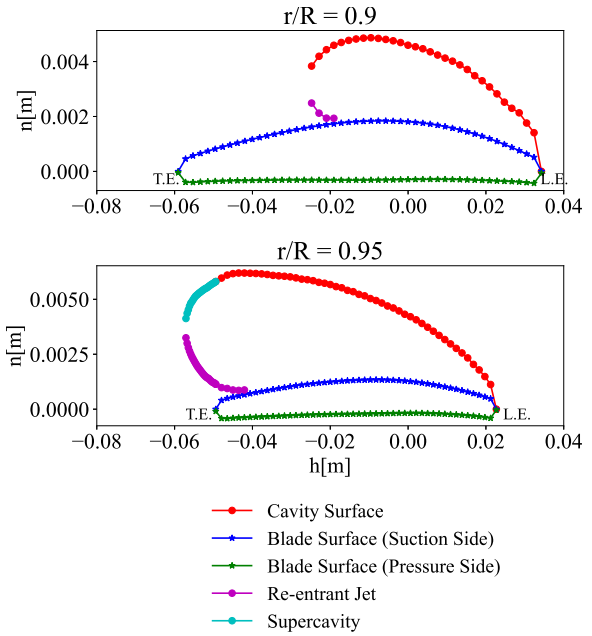

Figure 5: Blade surface and cavity surface geometries, represented in a blade-segment-fixed helicoidal coordinate system. h is the coordinate along the helical path of the blade segment. n is the coordinate normal to the helical path. Grid resolution intentionally made coarser.

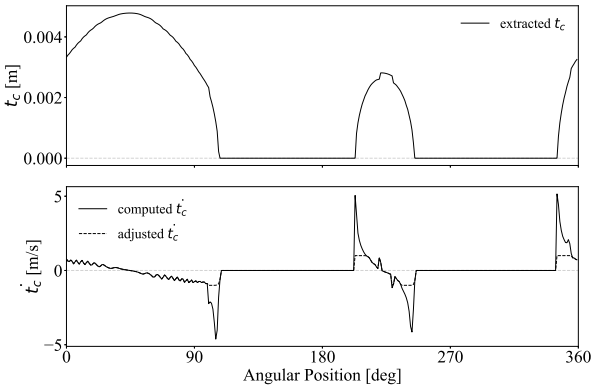

Figure 6: Modification of cavity thickness gradient - time history on a discrete panel

From the collection of data points for the blade and cavity segments, the discrete cavity thicknesses along the blade surface are to be extracted. A consistent definition of the cavity thickness is the offset of the cavity surface from the blade surface, along the blade surface normal. To facilitate this, the data points are converted to a helicoidal coordinate system ($h-n$) fixed on the individual blade segment, where the h axis represents the distance along the helix and n represents distances along the normal direction to the helical path (see Figure 5). The transfer of coordinates may be referred from chapter 14 of Breslin and Andersen (1993). From the point cloud for $h-n$ coordinates, a uniformly spaced grid is interpolated, and the discrete values of panel centroids are extracted.

In order to recreate the cavity surface thoroughly, the effects of supercavities and the re-entrant jet also need to be captured. Supercavitation occurs when the sheet cavity extends beyond the trailing edge of the blade segment. An example can be seen in Figure 4 for the radial segment $r/R = 0.95$ at the blade angular position 40 degrees. An additional set of grid points is defined beyond the trailing edge for supercavitating blade segments.

The re-entrant jet occurs at the trailing edge of the cavity, where fluid from the surrounding flow enters the cavity, detaching some part of the cavity from the blade surface. This can be seen for both the radial segments in Figure 4. The data points corresponding to the supercavity and the re-entrant jet are extracted separately, as can be seen in Figure 5. It is to be noted that the grid resolution in the figure is intentionally made coarser, in order to highlight the discretization process. The calculations are made with a finer grid resolution.

The cavity thickness (t_{c_i}) for a panel i, with centroid at helicoidal location h_i is the difference between the n coordinates of the cavity surface (n_{Cavity}) and blade surface (n_{Blade}). For grid points where the re-entrant jet is observed, the blade surface ordinate is replaced by the re-entrant jet surface ordinate (n_{Jet}). The normal velocity of the cavity surface is obtained as the time derivative of the cavity thickness. The procedure is summarized in Equation (2).

$$\begin{aligned} t_{c_i} &= n_{\text{Cavity}} - \max(n_{\text{Blade}}, n_{\text{Jet}}) \\ v_n &= \dot{t_c} \end{aligned} \tag{2}$$

Due to the dynamic nature of the cavity thickness, high gradients of the cavity thickness fluctuation are not accurately captured by Equation (2). This is particularly evident at the end of the cavity shrinkage phase and at the beginning of the cavity growth phase, as seen in Figure 6. This gives rise to spurious spikes in the acoustic model, which inadvertently amplifies the acoustic signal. The cavity normal velocity is adjusted by applying a threshold value to such limiting cases. It is to be noted that this error occurs only for a limited number of panels, but is sufficiently large to affect the integrated acoustic pressure. The extent of the modification is illustrated in Figure 6, which shows the time history of the most affected panel.

2.4 Coherence Check for Cavity Surface Extraction

As the cavity surface data are handled between multiple software platforms and multiple coordinate systems, a coherence check is undertaken in order to verify the data extraction procedure. Integral quantities pertaining to the cavity surface definition, namely the cavity surface area and the cavity surface volume, are calculated before and after the data extraction.

The cavity surface area in Star-CCM+ is calculated as the intersection area between the sheet cavity isovolume and the blade surface. The cavity volume is calculated as the volume of all cells that have a vapor-water volume fraction greater than 0.9. It is to be noted that tip vortex cavities are excluded from the isovolume by restricting the angular extent in the ϕ direction and the wall-distance of the cells.

Following data extraction, the cavity surface is calculated by integrating the panel areas of the cavitating panels at any given time step. The data extraction is done for radial sections from $r/R = 0.6$ to $r/R = 0.95$, with an increment of 0.05. The radial length of the panels is approximated as the mean-length between successive radial segments. The chord length is obtained from the segmental interpolation procedure along the helicoidal axis. Each blade segment is divided into 100 equally spaced panels. Panel areas are approximated as the product of their radial lengths and chord lengths. Cavity volume is obtained by integrating the cavity thickness over the panel areas.

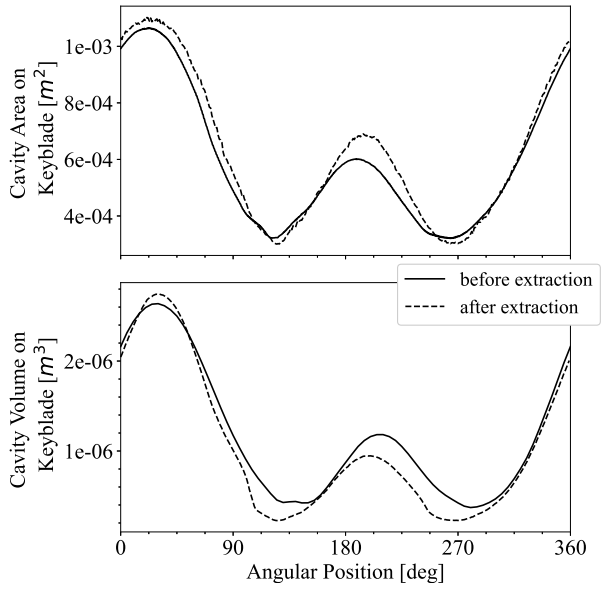

Figure 7: Comparison of Cavity Area and Volume. 'Before extraction' refers to quantities calculated in Star-CCM+. 'After extraction' refers to quantities calculated from the extracted values of cavity thickness, in DOLPHIN.

Figure 7 shows the comparative time history of the sheet cavity area and volume for a single-blade, before and after data extraction. The overall trend of cavity area and volume fluctuations, along with the order of magnitude, are well-retained after data extraction. However, an exact match is not achieved due to a variety of approximations involved in the cavity area and volume calculations. The values extracted from Star-CCM+ ('before extraction' in Figure 7) are based on a fine grid resolution. However the extracted data is on a coarser grid; a rectangular approximation is used to estimate the panel surface areas and trapezoidal integration used for the cavity volume. This can lead to discrepancies, particularly for panels close to the propeller tip. Nevertheless, the relative comparison of the cavity area and volume is performed only as a coherence check, and an exact fit is not expected. The general characteristics of the sheet cavity isovolume seem to be well-captured by the extraction process, and the information loss during the extraction process is within acceptable limits.

3 RESULTS AND EVALUATION

Despite its robustness and clarity in definition of the acoustic surface, the solid-FWH approach is currently less preferred than the permeable-FWH approach for cavitating propeller acoustics. The hybrid approach presented in the previous section aims to address this shortcoming of the solid-FWH approach, by extending its application to solid, impermeable cavity boundaries. In this section, the solid-FWH model for cavity surfaces is evaluated for its accuracy, applicability and limitations.

Since the solid-FWH acoustic model does not account for the turbulent broadband noise, the evaluation study is based on the comparison of the harmonics of the tonal noise. Initially, a verification study is conducted wherein the implementation of the solid-FWH acoustic model is checked with respect to a known solution. Since analytical solutions are rare for propeller cavitation acoustics, the verification study is done against a known hydrodynamic flow solution. Thereafter, the solution from the two acoustic models, namely the solid-FWH model in DOLPHIN and the permeable-FWH model in Star-CCM+, are compared against each other. Finally, the results are evaluated for their industrial applicability by comparing with cavitation tunnel and full-scale noise measurements.

3.1 Verification against Hydrodynamic Pressure Pulses

In an ideal scenario, verification against an existing analytical solution would have been the first step of evaluation. However, similar to many industrial flow applications, it is difficult to obtain a pertinent analytical case for propeller cavitation acoustics. Therefore, the verification philosophy is based on an understanding of the correlation between the hydrodynamic and hydroacoustic solutions for the propeller flow.

The hydrodynamic pressure field obtained from the DES solver is a solution to the incompressible, viscous Navier-Stokes equation. The hydroacoustic solution using the Farrassat1A formulation of the FWH acoustic analogy is obtained when the acoustic wave equation for a compressible flow field is solved for the acoustic pressure (i.e. fluctuating component of the pressure), but neglecting viscosity in the acoustic transmission process. Both solutions are obtained through reasonable simplifications to the compressible Navier-Stokes equation. In the context of the propeller sheet cavitation acoustic problem, the acoustic anal-

ogy uses noise sources based on the hydrodynamic solution on the sheet cavity surface. It should then be possible to correlate the hydrodynamic and hydroacoustic solutions at least in the near-field, where the compressibility effects are negligible. It is pertinent to mention that the correlations only exist with regards to the pressure pulses (or the fluctuating component of the unsteady pressure), since the hydroacoustic solution does not solve for the total pressure field.

The hypothesis used in this verification study is that the hydroacoustic pressure fluctuations for receiver points in the near-field are approximately equal to the hydrodynamic pressure fluctuations at these points. The near-field may be defined as points which are close enough to the acoustic source so that the speed of sound has no significant impact on the pressure at those points. The same verification philosophy has previously been used by Wang et al. (2020) during the evaluation of an acoustic analogy model for non-cavitating propellers.

On this basis, the hydrodynamic pressure pulse amplitudes in the free-field obtained in Star-CCM+ and those predicted by the acoustic models are compared. The time history of the hydrodynamic pressure includes high-frequency noise due to turbulence, for which the verification hypothesis is not valid. Hence, the comparison is done for pressure pulse amplitudes at multiples of blade passing frequency. The pressure pulse decay behaviour is analyzed for incremental distances along the vertical (z) direction, for points up to 10 times the propeller diameter, and for the first two blade harmonics, as seen in Figure 8. Higher harmonics are not included due to the possible influence of tip vortex cavitation on the hydrodynamic pressure pulses. Based on Berger (2018), an order of magnitude analysis of the tip vortex cavity fluctuations is conducted, and it is estimated for the present case that there are significant contributions from the tip vortex cavity between the 2nd and 3rd harmonics.

For the first harmonic, the pressure pulses predicted by both hydroacoustic models are at similar levels to the hydrodynamic pressure pulses in the near-field. Further into the far-field, the hydrodynamic pressure pulses decay at a faster rate than the hydroacoustic pressure pulses. This behaviour follows the same trend as predicted by Wang et al. (2020) and Ianniello (2016). In the far-field, the acoustic source behaves like a monopole, as seen in comparison with the reference line indicating monopole decay ($1/r$).

However, the agreement does not seem to be as consistent for the second harmonic pressure pulse decay behaviour. The permeable-FWH model underpredicts the higher harmonics, which can be possibly attributed to the uncertainty in the definition of the permeable data surface. The effect of tip vortex fluctuations are not captured by both acoustic models; hence, this can be ruled out as possible explanations. The results from the solid-FWH model are promising, with a similar kind of decay behaviour and consistency with the hydrodynamic pressure pulses as seen for the first harmonic. Consistent results were also obtained for decay along the horizontal direction, but are not included here for brevity. It is expected that the same behaviour extends for higher harmonics, if the solid-FWH model includes the tip vortex cavities as well.

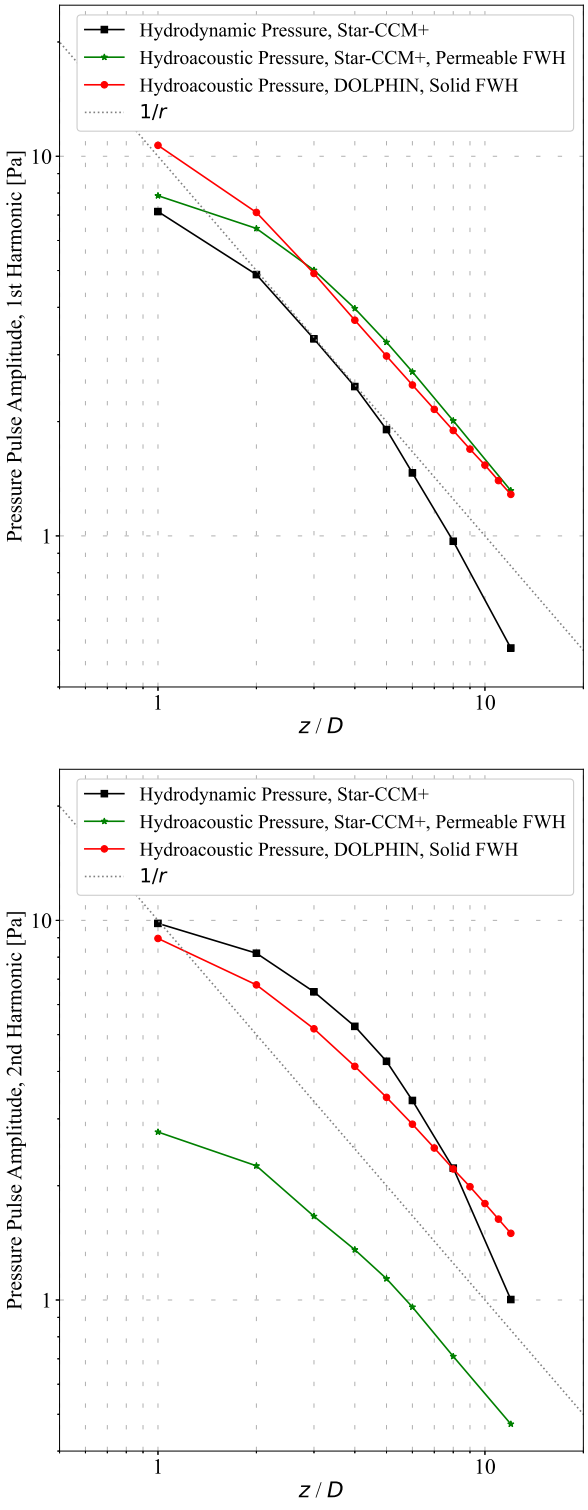

Figure 8: Comparison of hydrodynamic and hydroacoustic pressure pulse decay rates

3.2 Validation with Experimental Results

The best way to assess the relevance of a numerical acoustic approach is by validating it with experimental measurements. The cross-comparison of the simulation results with experimental results from existing literature is a formidable

task, riddled with uncertainties and in many cases it can only provide a superficial comparison. Nevertheless, a cross-comparison would give a qualitative indication about the strengths and limitations of the acoustic models.

A similar type of evaluation has previously been performed by Sezen and Atlar (2023) during the validation of their permeable-FWH model. The operating condition used within the current paper corresponds to test case 'C3' in Sezen and Atlar (2023). The experimental validation datasets used are: (i) model scale noise measurements from the University of Genoa (UNIGE) cavitation tunnel (Sezen and Atlar 2023) and (ii) full-scale noise measurements of the 'Princess Royal' vessel, conducted by the University of Southampton (Brooker and Humphrey 2016).

Firstly, all the comparison data is converted into full-scale noise spectra in 1/3rd octave bands as per the ITTC noise scaling procedure (ITTC 2017), using the exponent values for 'proportional bandwidth' and 'low frequency'. For the simulation data, the receiver point corresponding to hydrophone 'H1' (see Sezen and Atlar 2023) is used, similar to the procedure used in the cavitation tunnel data. The relative comparison between the two acoustic models and the experimental data is shown in Figure 9. The results from the permeable-FWH acoustic model used in Sezen and Atlar (2023) is also plotted for relative comparison. Only results up to the 6th harmonic frequency are included here, as the noise in higher frequencies is expected to have significant contributions from small-scale cavity structures and flow-induced turbulence.

The source levels from the permeable-FWH model in the current paper are of the same order as that published in Sezen and Atlar (2023). The differences at frequencies 200 to 500 Hz is possibly due to the restriction of the acoustic domain size in the current paper. Furthermore, the numerical predictions are lower compared to the model scale and full-scale measurements. This shows the likely influence of tip vortex cavitation induced noise, as the frequency range coincides with the order of magnitude estimation based on Berger (2018). The solid-FWH model seems to have predictions that are closer to the experimental results, as compared to the predictions from the permeable-FWH models. The solid-FWH model only predicts the noise at the blade harmonics; therefore, there are empty bins when converting the results to octave bands. Hence, the solid-FWH results are indicated by markers. Nonetheless, the seemingly better prediction of the acoustic source levels with the solid-FWH model in the experimental validation case is an encouragement to advance further research based on this implementation.

There is a notable discrepancy between the full-scale measurements and model-scale measurements, which points to the degree of uncertainty in the measurements. Tani et al. (2017) provides the comparison of the noise spectra from two testing facilities for the Princess Royal propeller (see Figure 32 to 36 of Tani et al. 2017), wherein deviations in the range of 5 to 10 dB are observed, for the same predetermined operating conditions. The sensitivity of the acoustic measurements to parameters such as the shaft revolution rate, cavitation number, mean thrust coefficient, and dissolved oxygen content are assessed by Tani et al. (2017), and all these contribute to the high uncertainty in acoustic measurements. The high level of uncertainty when validating with experimental data emphasises the need for prior verification studies of noise prediction simulations. A qualitative verification of the decay behaviour with the hydrodynamic pressure pulses, as performed in Section 3.1, can be a useful evaluation tool in this regard.

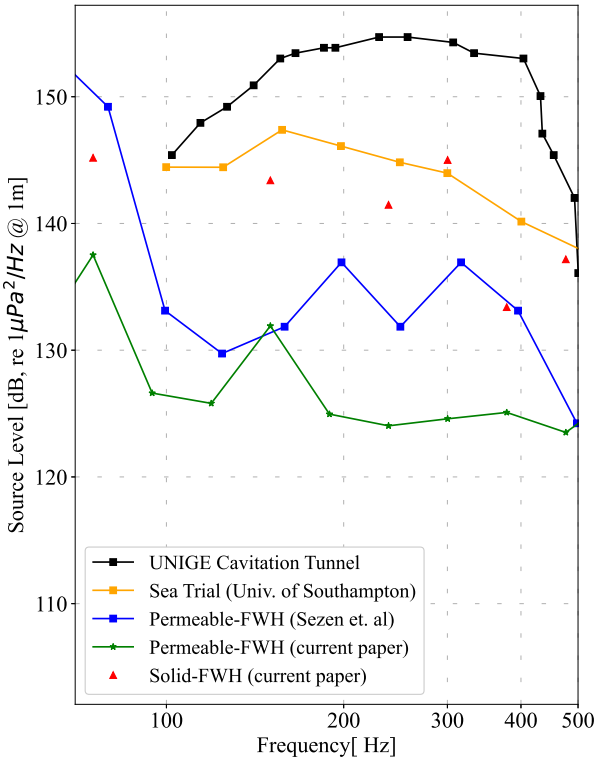

Figure 9: Validation with experimental data, in 1/3rd octave bands

4 CONCLUSION

The relevance of the solid-FWH implementation in propeller hydroacoustics is based on its unambiguous definition of the data surfaces. In this paper, the cavity surface is extracted based on the flow results from a VOF solver, within a reasonable level of approximation. However, the verification and validation of the predicted hydroacoustic pressure faces many challenges.

Firstly, the hydrodynamic pressure is a combination of the contribution of all flow phenomena present in the simulation domain. This includes the blade rotation, sheet cavities, tip vortex cavities and the influence of flow turbulence. The current implementation of the solid-FWH model includes only sheet cavities. The effect of tip vortex cavitation could influence the lower harmonics, particularly for low cavitation number operating conditions, where the characteristic tip vortex fluctuation frequencies are much lower (Berger 2018). In order to truly evaluate the solid-FWH model, an equivalent acoustic model for tip vortex cavities is also to be included.

Secondly, the uncertainty in validating acoustic results with experimental data is to be highlighted. The sources of un-

certainty can broadly be categorized into (i) uncertainty in the test setup, (ii) uncertainty in the noise calculation procedure, and (iii) uncertainty in the noise phenomena. Uncertainty in the test setup includes the scale effects, the effect of background noise and the effect of acoustic reflections. It is difficult, and sometimes impractical, to account for all these effects in numerical simulations. The uncertainty in the noise calculation procedure stems from the different methods in which the acoustic results can be presented - in time domain or frequency domain, in 1/3rd octave bands or as narrow-band spectra, as equivalent source levels or as sound pressure levels, to name a few distinctions. The ISO 17208 standards (ISO 17208 2019) aims to address this by standardizing the noise representation data. However, publications in such standardized representations lead to a loss of useful information, such as the tonal noise and the directivity effect on the noise spectrum. The uncertainty in noise phenomena refers to the dominating noise mechanism for the operating condition considered, and for the frequency range of interest. One drawback of Navier-Stokes equation based acoustic solvers is that the contribution from different noise sources cannot be separated. Solid-FWH based acoustic analogy based solvers are more efficient in this aspect, by being able to separately quantify the noise due to blade rotation, due to cavity fluctuations and due to turbulence. However, the verification and validation of such an approach needs further investigation beyond what has been attempted in the current paper - for multiple operating conditions and multiple propeller geometries.

Future work is aimed at extending the verification and validation study of the solid-FWH model, by including the effects of tip vortex cavitation and investigating multiple operating conditions. With promising results from the current investigation, the cavity surface data extraction can be attempted on a finer resolution grid, to improve the accuracy of the method. A holistic comparison between the permeable-FWH and solid-FWH models, particularly the effect of the acoustic domain size and shape in the permeable-FWH model, could also provide insight into their respective applicability in industrial cavitation acoustics problems.

REFERENCES

Ahmed, S. (2020). On the noise generated by a ship propeller. PhD thesis, University of New South Wales.

Berger, S. (2018). Numerical Analysis of Propeller-Induced Higher-Order Pressure Fluctuations on the Ship Hull. PhD thesis, Hamburg University of Technology, Hamburg.

Brentner, K. S. and Farassat, F. (2003). Modeling aerodynamically generated sound of helicopter rotors. Progress in Aerospace Sciences, 39(2-3):83–120.

Breslin, J. P. and Andersen, P. (1993). Hydrodynamics of Ship Propellers. Cambridge Ocean Technology Series. Cambridge University Press.

Brooker, A. and Humphrey, V. (2016). Measurement of radiated underwater noise from a small research vessel in shallow water. Ocean Engineering, 120:182–189.

Ffowcs-Williams, J. E. and Hawkings, D. L. (1969). Sound generation by turbulence and surfaces in arbitrary motion. Philosophical Transactions of the Royal Society of London. Series A, Mathematical and Physical Sciences, 264:321–342.

Göttsche, U., Scharf, M., Berger, S., and Abdel-Maksoud, M. (2017). A hybrid numerical method for investigating underwater sound propagation of cavitating propellers. In Sixth International Symposium on Marine Propulsors (smp'19), volume 3, Espoo, Finland. VTT Technical Research Centre of Finland Ltd.

Ianniello, S. (2016). The Ffowcs-Williams–Hawkings equation for hydroacoustic analysis of rotating blades. Part 1.-The rotpole. Journal of Fluid Mechanics, 797:345–388.

ISO 17208 (2019). Underwater acoustics - quantities and procedures for description and measurement of underwater sound from ships. Standard, International Organization for Standardization, Geneva, CH.

ITTC (2017). The Specialist Committee on Hydrodynamic Noise. Technical report, International Towing Tank Conference, Wuxi, China.

Lidtke, A., Lloyd, T., and Vaz, G. (2019). Acoustic modelling of a propeller subject to non-uniform inflow. In Sixth International Symposium on Marine Propulsors, Rome, Italy.

Sezen, S. and Atlar, M. (2023). Marine propeller underwater radiated noise prediction with the FWH acoustic analogy Part 2: Assessment of model scale propeller hydroacoustic performance under non-uniform flow conditions. Ocean Engineering, 270:113443.

Shin, K. and Andersen, P. (2019). CFD analysis of ship propeller thrust breakdown. In Sixth International Symposium on Marine Propulsors (smp'19), Rome, Italy.

Shin, K., Tomy, J. P., Berger, S., Lundgren, E., and Nielsen, J. R. (2023). CFD prediction of ship propeller-induced underwater radiated noise. In Proceedings of InterNoise 2023, Chiba, Japan.

Shin, K. W., Regener, P. B., and Andersen, P. (2015). Methods for cavitation prediction on tip-modified propellers. In Fourth International Symposium on Marine Propulsors, Austin, Texas, U.S.A.

Tani, G., Aktas, B., Viviani, M., and Atlar, M. (2017). Two medium size cavitation tunnel hydro-acoustic benchmark experiment comparisons as part of a round robin test campaign. Ocean Engineering, 138:179–207.

Testa, C. (2008). Acoustic Formulations for Aeronautical and Naval Rotorcraft Noise Prediction Based on the Ffowcs Williams and Hawkings Equation. PhD thesis, Università degli Studi Roma Tre, Rome.

Wang, Y., Göttsche, U., and Abdel-Maksoud, M. (2020). Sound field properties of non-cavitating marine propellers. Journal of Marine Science and Engineering, 8:855.